Title

Helicobacter pylori Chronic-Stage Inflammation Undergoes Fluctuations That Are Altered in tlpA Mutants

Journal

Infection and Immunity, 91(1)

ISSN

0019-9567

Authors

Johnson, Kevin S
Yang, Christina
Carter, J Elliot
et al.

Publication Date

2023-01-24

DOI

10.1128/iai.00322-22

Peer reviewed

AMERICAN SOCIETY FOR MICROBIOLOGY | Infection and Immunity®

HOST RESPONSE AND INFLAMMATION

Helicobacter pylori Chronic-Stage Inflammation Undergoes Fluctuations That Are Altered in *tlpA* Mutants

Kevin S. Johnson,[a] Christina Yang,[a] J. Elliot Carter,[b] Atesh K. Worthington,[c,d] Elektra K. Robinson,[c] Raymond Lopez-Magaña,[a] Frida Salgado,[a] Isabelle Arnold,[e] Karen M. Ottemann[a]

[a]Department of Microbiology and Environmental Toxicology, University of California Santa Cruz, Santa Cruz, California, USA
[b]Department of Pathology, University of South Alabama College of Medicine, Mobile, Alabama, USA
[c]Department of Molecular, Cellular, and Developmental Biology, University of California Santa Cruz, Santa Cruz, California, USA
[d]Institute for the Biology of Stem Cells, University of California-Santa Cruz, Santa Cruz, California, USA
[e]Institute of Experimental Immunology, University of Zürich, Zürich, Switzerland

ABSTRACT *Helicobacter pylori* colonizes half of the world's population and is responsible for a significant disease burden by causing gastritis, peptic ulcers, and gastric cancer. The development of host inflammation drives these diseases, but there are still open questions in the field about how *H. pylori* controls this process. We characterized *H. pylori* inflammation using an 8-month mouse infection time course and comparison of the wild type (WT) and a previously identified mutant lacking the TlpA chemoreceptor that causes elevated inflammation. Our work shows that *H. pylori* chronic-stage corpus inflammation undergoes surprising fluctuations, with changes in Th17 and eosinophil numbers. The *H. pylori tlpA* mutant changed the inflammation temporal characteristics, resulting in different inflammation from the wild type at some time points. *tlpA* mutants have equivalent total and gland colonization in late-stage infections. During early infection, in contrast, they show elevated gland and total colonization compared to those by WT. Our results suggest the chronic inflammation setting is dynamic and may be influenced by colonization properties of early infection.

KEYWORDS chemoreceptors, chemotaxis, chronic infection, gastric, gut inflammation

Inflammation underlies a widespread set of disease states, resulting from diverse triggers that can be abiotic or microbial. In healthy inflammation, the inflammatory response is triggered and then resolves. Some triggers, however, result in chronic inflammation that does not fully resolve, resulting in lifelong disease. One such trigger is the bacterium *Helicobacter pylori*. This bacterium colonizes individuals often during early childhood and maintains a lifelong colonization of the stomach (1, 2). Colonization in the very early childhood period leads to immunological benefits, characterized by the development of regulatory T cells (Tregs) that in turn decrease the risk of asthma and other pathologies (1, 3, 4). Continued colonization into later life, however, can lead to disease, including gastritis, peptic ulcers, and gastric cancer, ultimately contributing to a significant disease burden throughout the world (3, 5–7). These diseases arise from *H. pylori*-driven stomach inflammation. To be able to control these diseases, it is critical to understand the mechanisms by which this bacterium manipulates host inflammation.

H. pylori forms intimate interactions with the mammalian host, colonizing two distinct regions of the stomach called the corpus and antrum. *H. pylori* is found in several locations, including in the mucus layer lining the gastric epithelium, attached to gastric epithelial cells, and within gastric glands that invaginate both regions (8–11). By all accounts, the stomach does not appear to be a hospitable niche for colonization. Its high acidity is toxic to *H. pylori* (12), and contents of the stomach are emptied within hours of eating a solid digestible meal (13). In addition, the mucus layer (14, 15) and

Editor Nancy E. Freitag, University of Illinois at Chicago

Address correspondence to Karen M. Ottemann, ottemann@ucsc.edu.

The authors declare no conflict of interest.

Received 1 August 2022
Returned for modification 30 August 2022
Accepted 27 November 2022
Published 19 December 2022

gastric epithelial cells are renewed in a matter of days, a process which is exacerbated by *H. pylori* colonization (16, 17). Despite these challenges, *H. pylori* chronically colonizes the stomach using a variety of factors. These include virulence factors such VacA and γ-glutamyl-transpeptidase (GTT), which both lead to tolerogenic T-cell responses through effects on myeloid cell populations in the stomach (2, 18), the Cag pathogenicity island (PAI), which alters host cell signaling, increasing host inflammation and disease severity, adherence factors to facilitate host cell attachment, and urease to buffer the local environment of the bacteria, as well as several other factors (2, 9).

H. pylori locates to specific regions in the stomach, in a manner that is dictated by its chemotaxis system (19). Chemotaxis regulates bacterial motility in response to harmful and beneficial signals. These signals are sensed by chemoreceptors and are transduced through a two-component signal transduction system (9, 20). *H. pylori* expresses four chemoreceptors, TlpA, TlpB, TlpC, and TlpD. Much work has been done to determine the sensing profile of these chemoreceptors and their roles *in vivo*. Multiple attractants are sensed that are beneficial for *H. pylori* growth, including arginine, fumarate, and cysteine by TlpA, urea by TlpB, and lactate by TlpC (21–25). Repellents, in contrast, are harmful to the bacteria and include acid sensed by multiple chemoreceptors, autoinducer-2 sensed by TlpB, and reactive oxygen species (ROS) sensed by TlpD (26–30). The ability to sense signals chemotactically is critical for *in vivo* gland colonization, as chemotaxis and chemoreceptor mutants exhibit significant gastric gland colonization defects *in vivo* (8, 28, 31, 32). Ultimately, chemotaxis maximizes the fitness of the bacteria *in vivo*, as essential metabolites can be sought, and harmful host conditions can be avoided.

H. pylori chemoreceptors play unique roles during colonization, likely due to their distinct sensing profiles. Some in *H. pylori* promote colonization levels, while others affect inflammation. This work focuses on TlpA, which is required for inflammation control. Specifically, Δ*tlpA H. pylori* induced significantly more inflammation, measured by histology at 6 months postinfection (33). At this time point, the Δ*tlpA* mutant does not differ from the wild type (WT) in colonization levels, although at earlier time points it does have a mild colonization defect in both single-strain and competition murine infections (34, 35). Intriguingly, the high inflammation phenotype associated with loss of TlpA was observed only at 6 months postinfection but not at 3 months (33). These results suggest loss of *tlpA* creates an *H. pylori* strain that has subtly altered host interactions. Given that host inflammation control by *H. pylori* dictates disease severity, this study aims to understand how TlpA modulates host inflammation (36–38).

Inflammation induced by *H. pylori* is initiated by bacterial interactions with innate immune cells, which in turn drive effector $CD4^+$ T-cell differentiation through the production of cytokines (18). Infection recruits myeloid cells to the gastric lamina propria. These cells include neutrophils, eosinophils, multiple types of dendritic cells (DCs), including $CD103^+$ $CD11b^+$ DCs, $CD103^+$ $CD11b^-$ DCs, and $CD103^-$ $CD11b^+$ DCs, and multiple types of monocytes and macrophages, including major histocompatibility class II-negative ($MHCII^-$) monocytes, $MHCII^+$ monocytes, and $MHCII^+$ macrophages (18, 39–41). These innate immune cell populations interact with and/or phagocytose *H. pylori*, leading to the recruitment of $CD4^+$ effector T cells. At the later stages of infection, the *H. pylori*-induced inflammation consists of large populations of $CD4^+$ effector T cells, including Th1, Th17, and Tregs (42). Th1 and Th17 cells promote proinflammatory responses by producing gamma interferon (IFN-γ) and interleukin-17a (IL-17a), respectively (36, 43–46). Conversely, Tregs suppress inflammation through the secretion of IL-10 (4, 36, 44–46). Overall, the inflammatory response induced by *H. pylori* consists of a mixture of pro- and anti-inflammatory T cells, as well as multiple types of innate immune cells.

The ability of *H. pylori* to colonize gastric glands is important for several reasons. For one, gland colonization seems to underlie colonization resistance, the property of an initial infection preventing a second one. Specifically, nonchemotactic *H. pylori* does not colonize the glands and develop colonization resistance like the WT does (32, 47, 48).

Second, *H. pylori* in the glands can interact with gastric Lgr5$^+$ stem cells, increasing the proliferation rate of these mammalian cells, leading to hyperplasia (17). Lastly, gland populations may be associated with inflammation. Specifically, nonchemotactic mutants do not colonize glands and induce significantly less inflammation (33, 46). This inflammatory response is associated with a decreased proinflammatory Th17 cell response compared to WT *H. pylori* (46). These data suggest that gland colonization may promote a proinflammatory Th17 response. Other data show that, in addition, the host T-cell response limits *H. pylori* gland infection, further supporting the connection (47, 49). Currently, it is unknown what role TlpA plays in gland colonization or how any phenotypes relate to host inflammation.

In this work, we aimed to better understand the characteristics of *H. pylori* inflammation by assessing gland and total colonization, as well as inflammation development over an 8-month infection course. We compared wild-type *H. pylori* to the *tlpA* mutant, to gain insight into inflammation control. We report the surprising finding that *H. pylori* chronic-stage inflammation is not constant and instead showed regular fluctuations, particularly in the corpus region. The *tlpA* mutant showed offset and enhanced inflammation compared to that of the WT. These inflammation variations were associated with changes in Th17 cell density. While there were some cooccurring colonization variations, the most substantial colonization differences between the WT and the *tlpA* mutant occurred in early infection, with *tlpA* required to maintain WT-level gland loads during early infection. This work suggests that bacterial properties, influenced by TlpA, affect host inflammation in the corpus by attenuating Th17 cell abundance, potentially through the regulation of early gland colonization.

RESULTS

***tlpA* mutants result in high fluctuating inflammation that is corpus specific and offset from WT inflammation.** Previous work showed that Δ*tlpA H. pylori* mutants induce high levels of inflammation at 6 months postinfection but normal levels at 3 months (33). We thus examined the inflammation kinetics of the WT and *tlpA* mutants. We carried out two independent, 8-month mouse colonization studies, orally infecting mice with WT or Δ*tlpA* SS1 green fluorescent protein-positive (GFP$^+$) *H. pylori*. Of note, this *tlpA* mutant is a clean, unmarked deletion that is distinct from the allele used previously (33) and the strain makes use of the stable plasmid pTM115 for GFP expression (32). Inflammation was assessed by histology of hematoxylin-and-eosin-stained tissue sections spanning the corpus to antrum. Inflammation grades were assigned by a pathologist (J. Elliot Carter) assessing the density and distribution of lymphocytic infiltration into the lamina propria of the corpus and antrum separately in samples that were used in a blind manner (33, 35). Inflammation grades, determined for both time courses, showed consistency in terms of a general increase in the first 2 months, and fluctuations in the later stages, as discussed below (see Fig. S1 in the supplemental material), and so are presented as averages (Fig. 1).

Consistent with previous work, *tlpA* mutants caused heightened inflammation around 5 to 6 months postinfection (Fig. 1A). Previous analysis did not dissect whether the *tlpA* inflammation was localized (33), and here we find that the elevated inflammation was restricted to the corpus and did not occur in the antrum (Fig. 1). Surprisingly, the *tlpA* inflammation showed periodic variations, with high inflammation points followed by low ones (Fig. 1A). These fluctuations were most prominent in the corpus, compared with the antrum (Fig. 1). When this inflammation profile was compared to that of the WT, we found that WT infections also displayed inflammation periodicity in the corpus but not the antrum (Fig. 1). Indeed, the elevated inflammation of *tlpA* mutants appeared due to a rapid rise in inflammation after 4 months of infection. The WT had a similar response, but at a slightly later time. This offset resulted in the *tlpA* mutant inflammation exceeding that of the WT at some times, e.g., 5 and 6.5 months. Due to the fluctuating nature, however, WT inflammation was greater than that of the *tlpA* mutant at other times, e.g., 5.5 months. The *tlpA* mutant corpus inflammation showed a greater range than that of the WT in the period 4 months postinfection. The *tlpA* mutant scores ranged from 0.9 to 2.3, while the WT scores

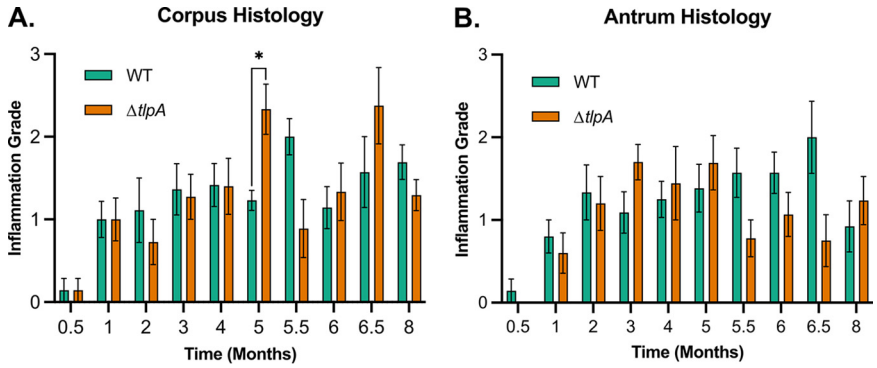

FIG 1 Δ*tlpA H. pylori* infections result in inflammation peaks with offset kinetics compared to those of the WT. Female C57BL/6N mice ($n \geq 7$ per group) were orally infected with the WT SS1 GFP$^+$ strain or the Δ*tlpA* SS1 GFP$^+$ strain for 0.5, 1, 2, 3, 4, 5, 5.5, 6, 6.5, and 8 months, in two independent infections. Inflammation induced by WT SS1 GFP$^+$ or Δ*tlpA* SS1 GFP$^+$ infection was measured by assessing lymphocyte recruitment to the lamina propria of corpus (A) and antrum (B) via histology, as described in Materials and Methods (33). Atrophy was not detected in any samples. Error bars represent the standard error of the mean. *, $P < 0.05$, comparisons between strains at the same time point using two-way ANOVA, Šídák multiple-comparison test.

ranged only from 1.5 to 2.0. The antrum inflammation was different. In this case, both the WT and the *tlpA* mutant had similar increasing trends from 0.5 to 5 months. After that, the WT mostly continued to increase slightly, while the *tlpA* mutant declined between 5 and 5.5 months and then remained at this new lower level. Overall, these results suggest that the corpus and antrum have somewhat different inflammation processes, with the corpus displaying periodic variations of high and low inflammation grades. The *tlpA* mutant causes elevated inflammation, with top scores that are higher than those of the WT, but also offset fluctuation kinetics.

Increased Th17 cell density is observed in Δ*tlpA H. pylori*-infected corpus during late infection. We next sought to better understand the nature of the periodic corpus immune responses, using flow cytometry to assess innate immune and effector T-cell populations in the samples from time course 1 (Fig. S1). On the innate immune side, we examined three types of DCs (CD103$^+$ CD11b$^+$ DCs, CD103$^+$ CD11b$^-$ DCs, and CD103$^-$ CD11b$^+$ DCs), two types of monocytes (MHCII$^-$ monocytes and MHCII$^+$ monocytes), MHCII$^+$ macrophages, neutrophils, and eosinophils, as described in previous work (39–41) (Fig. S2A). There were elevated numbers of these innate immune populations relative to uninfected animals (Fig. S3), but the populations mostly did not show patterns of temporal variation or substantial differences between WT and Δ*tlpA H. pylori* infection groups (Fig. 2). An exception was eosinophils, which were lower in WT infections at 6 and 8 months postinfection (Fig. 2A), although there was not lower WT inflammation at these time points (Fig. 1). Total numbers of eosinophils, however, did not always coincide with differences in percent CD45 frequency (Fig. S3). These results suggest the inflammation score fluctuation does not correlate with differences in the abundance of innate immune cell populations.

We next examined the CD4$^+$ effector T-cell populations, which are known to be key drivers of *H. pylori* inflammation (36, 43–46). Total CD4$^+$ effector T cells (CD4$^+$ T-cell receptor β positive [TCRβ^+]), as well as each subset, were assessed by the measurement of specific cell markers: Th1 (Tbet$^+$), Th17 (RorγT$^+$), and Treg (FoxP3$^+$) (Fig. S2B). These cell types were all elevated in mice infected with either WT or *tlpA* mutant *H. pylori*, compared to uninfected mice, with numbers steadily increasing by 10-fold over the time course (Fig. S4). At the 5-month time point, there were more Th17 cells than other types, but by 8 months, all three T-cell subsets were found in equal amounts (Fig. 3 and Fig. S4). There was some evidence of periodic fluctuation in cell amounts. At 5 months and 8 months postinfection, Th17 cells were significantly elevated in the Δ*tlpA H. pylori*-infected mice compared to the WT-infected mice (Fig. 3B). Th1 cell numbers also showed some periodicity, with peaks at 6 and 8 months. Treg numbers, in contrast, did not show variation and were consistently equivalent between the WT and

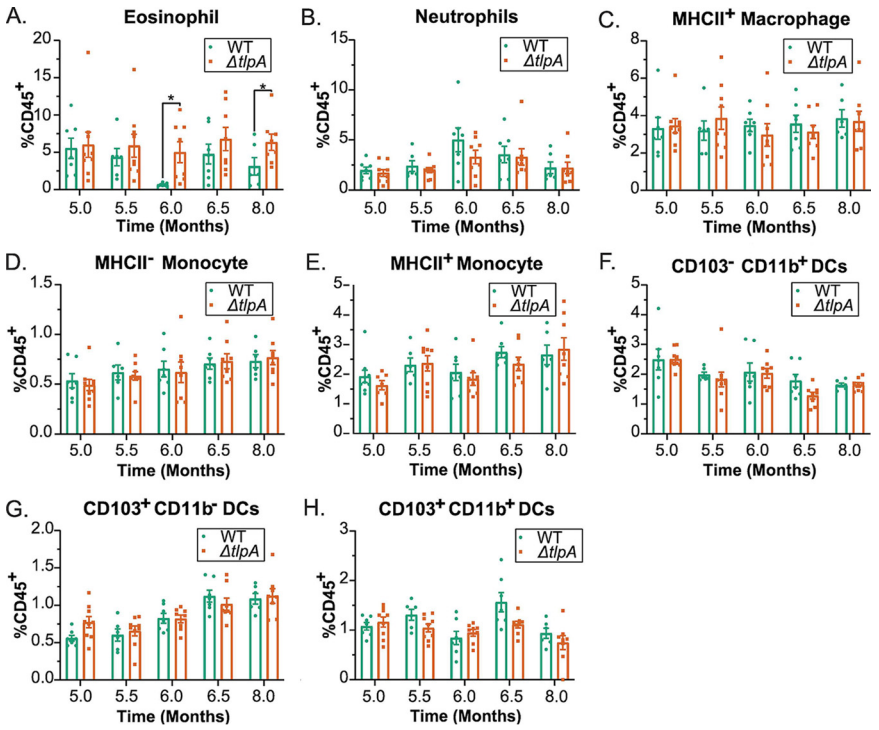

FIG 2 Innate immune cell recruitments during chronic infection are similar between WT SS1- and Δ*tlpA H. pylori*-infected mice. Mice infected with the WT SS1 GFP$^+$ or Δ*tlpA* SS1 GFP$^+$ strain were used to isolate corpus lamina propria leukocytes after 5, 5.5, 6, 6.5, and 8 months postinfection from the same mice as shown in Fig. S1A in the supplemental material (n = 7 to 9 per group from one experiment). The analysis including uninfected mice is included in Fig. S2. Eosinophils (A), neutrophils (B), MCHII$^+$ macrophages (C), MCHII$^-$ monocytes (D), MHCII$^+$ monocytes (E), CD103$^-$ CD11b$^+$ DCs (F), CD103$^+$ CD11b$^-$ DCs (G), and CD103$^+$ CD11b$^+$ DCs (H) were analyzed by flow cytometry. Data are presented as the frequency of each cell type as the percentage of all live CD45$^+$ lymphocytes. Error bars represent the standard error of the mean. *, $P < 0.05$, comparisons between strains using two-way ANOVA, Šídák multiple-comparison test.

the mutant (Fig. 3A and C). Overall, these results suggest that some T cells may undergo periodic fluctuation, possibly accounting for the heightened inflammation grade of *tlpA* mutants at 5.5 months. There are not, however, dramatic changes in T-cell counts between time points and strains.

Gland colonization patterns of *H. pylori* are dynamic throughout a long-term infection. Our analysis in Fig. 1 shows that *H. pylori* corpus inflammation undergoes periodic fluctuations during late infection stages, and these fluctuations are location specific. Because inflammation is driven by *H. pylori* presence, we next analyzed *H. pylori* colonization

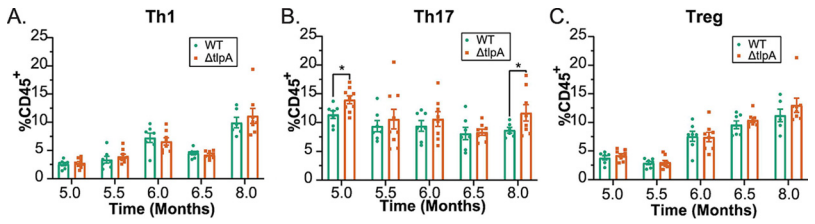

FIG 3 Δ*tlpA H. pylori*-infected mice display increased Th17 cell populations recruited to the corpus lamina propria. Mice were infected with the WT SS1 GFP$^+$ or Δ*tlpA* SS1 GFP$^+$ strain, and lymphocytes from the corpus lamina propria were isolated at 5, 5.5, 6, 6.5, and 8 months postinfection from the same mice from the experiment in Fig. 2 (n = 7 to 9 per group, from one experiment). The analysis including uninfected mice is included in Fig. S3 in the supplemental material. Th1 cells (Tbet$^+$ TCRβ^+ CD4$^+$) (A), Th17 cells (RorγT$^+$ TCRβ^+ CD4$^+$) (B), and Tregs (FoxP3$^+$ TCRβ^+ CD4$^+$) (C) were analyzed by flow cytometry. Data are presented as the frequency of each cell type as the percentage of all live CD45$^+$ lymphocytes. Error bars represent the standard error of the mean. *, $P < 0.05$, comparisons between strains using two-way ANOVA, Šídák multiple-comparison test.

levels and patterns. Previous work had assessed the total tissue colonization of both WT and *tlpA* mutant strains (33–35), but since that initial analysis, there has been increased appreciation that *H. pylori* is found in multiple microniches, including within and outside gastric glands and between the corpus and antrum (8, 28, 32). Accordingly, we assessed the colonization patterns of WT and Δ*tlpA* SS1 GFP$^+$ *H. pylori* from the time course samples above (Fig. 1). At each time point, we enumerated corpus and antrum total CFU from bulk tissue and then multiple gland parameters including the average number of bacteria per gland (gland colonization), the average number of bacteria per occupied gland (gland density), and the percentage of glands occupied (gland percent) (Fig. 4). Of note, gland colonization is the composite of both gland density and gland percent, thus providing an overall picture of gland colonization dynamics, e.g., how gland colonization varied over time. The latter two metrics give contextual understanding to the overall gland colonization patterns. Colonization and gland data were analyzed from both time courses, showing similar trends as noted below. Because time course 1 has more time points, it is shown in Fig. 4 and 5, with time course 2 shown in the supplemental material.

As reported previously, WT *H. pylori* initially colonizes the antrum to a higher level than the corpus during the first ~1 month of infection, and then antral numbers decline such that there are not significant differences in the total number of bacteria between these regions (Fig. 4A) (32, 48, 50). Δ*tlpA* mutants displayed a similar pattern (Fig. 4E), with two notable differences. First, the corpus CFU were elevated at 1 month postinfection compared to the WT value (Fig. 5A), and the early decline in antral numbers was more dramatic (Fig. 5E). The second time course captured time points only after 2 months of infection and was consistent with the first time course in not detecting significant differences between the WT and the mutant in terms of CFU (Fig. S5). Overall, these bulk tissue analyses support previous findings that the *tlpA* mutant does not have substantial colonization defects and indeed may even colonize to slightly higher levels in the corpus in early infections.

We next analyzed the gland populations. Similarly to previous reports, the WT colonized ~30 to 50% of the glands by 2 weeks (Fig. 4D), with ~20 bacteria per gland in both the corpus and the antrum (Fig. 4B and C) (32). Antral gland colonization expanded during the next 2 weeks (Fig. 4B). The percentage of glands occupied increased to ~70%, and the number of bacteria per occupied gland increased to ~30 (Fig. 4C and D). In contrast, the corpus gland populations remained steady (Fig. 4B to D). After this expansion period, antral gland colonization showed an abrupt decline between months 1 and 3 (Fig. 4B; Fig. S5). This decline was mostly due to a significant decline in the number of bacteria per gland, while the percentage of occupied glands remained high (Fig. 4C and D). The corpus, in contrast, retained a steady number of bacteria per occupied gland at ~20 and declined only in the percentage of glands occupied, down to ~15%. During this same period, we observed multiple differences between the WT and the *tlpA* mutant. The most noticeable difference was that the *tlpA* mutant colonized the corpus glands to higher levels than did the WT in early infection. In the first month, Δ*tlpA H. pylori* showed elevated numbers associated with high bacterial numbers per gland and sometimes a high percentage of occupied glands (Fig. 5C and D).

From 2 to 8 months postinfection, there were few differences in gland colonization between the strains in either the corpus or the antrum, in both time courses (Fig. 5B and F; Fig. S5). For both strains, gland colonization decreased from the peak at 1 month postinfection over the remainder of the infection (Fig. 5B and F). There was an increase in both WT and Δ*tlpA H. pylori* gland colonization at 4 months in one time course (Fig. 4) but not the other (Fig. S4). Δ*tlpA H. pylori* consistently colonized fewer glands than did the WT in both regions, achieving significance in many instances (Fig. 5D and H; Fig. S5). One exception to this pattern was at 5.5 months postinfection in the antrum when Δ*tlpA H. pylori* had significantly higher gland percent occupancy (Fig. 5H) and a nonsignificant increase in gland density (Fig. 5G). A similar increase was also detected in time course 2 at the 6-month infection time point (Fig. S5).

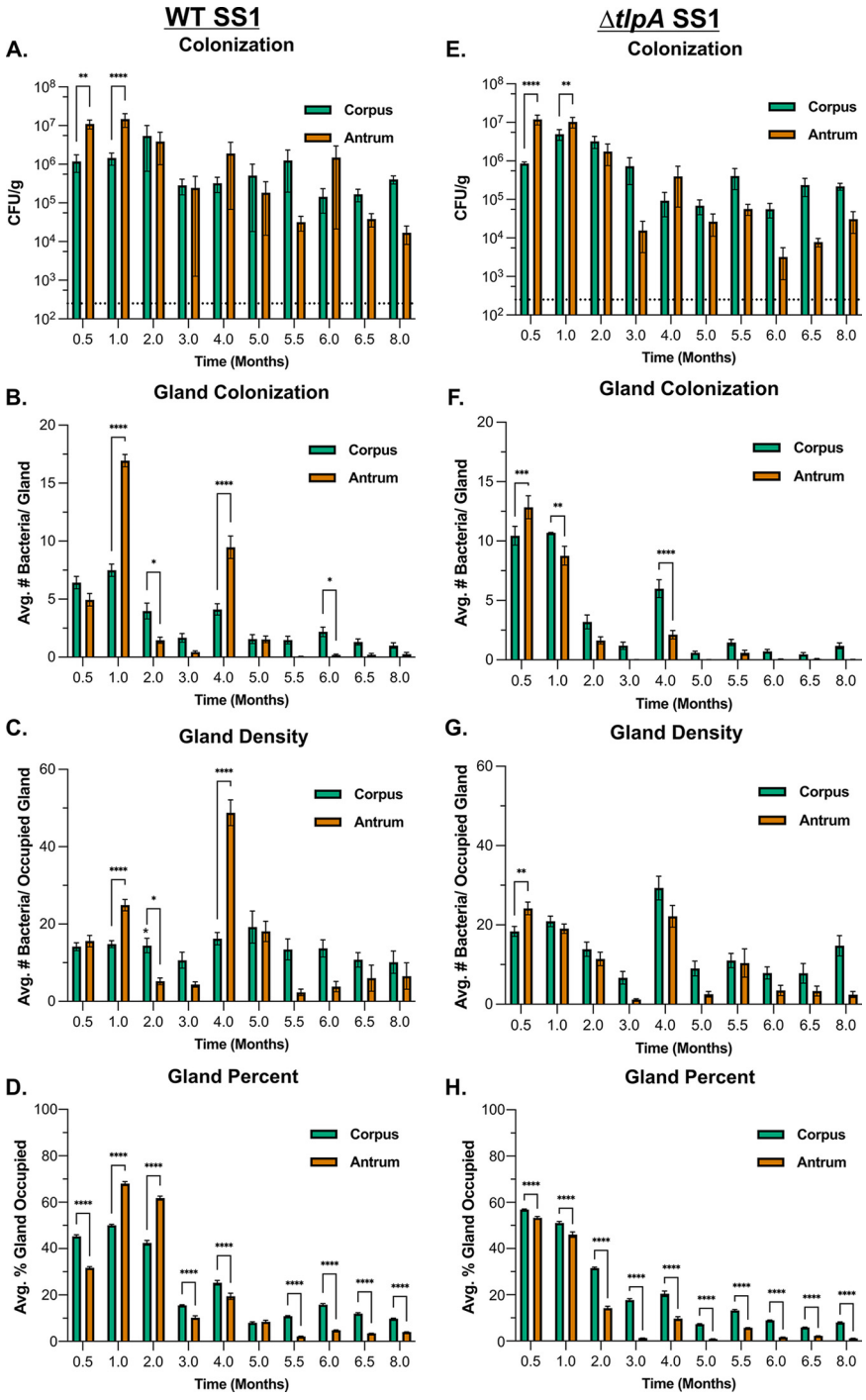

FIG 4 WT SS1 and Δ*tlpA H. pylori* SS1 have defined colonization patterns in the murine stomach. Colonization patterns of WT SS1 and Δ*tlpA* SS1 within the mouse stomach were analyzed over a time course from the acute to chronic stage of infection from the same mice from Fig. S1A and B, time course 1, in the supplemental material. Female C57BL/6N mice ($n \geq 4$) were orally infected with the WT SS1 GFP$^+$ or Δ*tlpA* SS1 GFP$^+$ strain for 0.5, 1, 2, 3, 4, 5, 5.5, 6, 6.5, and 8 months. (A and E) Total colonization levels of WT (A) and Δ*tlpA* (E) strains in the corpus and antrum region of the stomach were determined by homogenizing tissue and plating for CFU. For each strain, gland colonization phenotypes were quantified and compared between the corpus and antrum. Individual glands were isolated, and GFP$^+$ bacteria were visualized using the Bacterial Localization in Isolated Glands (BLIG) method (32). For each mouse, 100 isolated glands from the corpus and 100 from the antrum were analyzed. (B and F) Gland colonization is the average number of WT SS1 GFP$^+$ or Δ*tlpA* SS1 GFP$^+$ bacteria per all glands analyzed in either region. (C and G) Gland density is the average number of WT SS1 GFP$^+$ or Δ*tlpA* SS1 GFP$^+$ bacteria per occupied gland. (D and H) Gland percent is the average percentage of glands that are occupied by either the WT SS1 GFP$^+$ or the Δ*tlpA* SS1 GFP$^+$ strain at each time point. For all graphs, error bars represent the standard error of the mean. *, $P < 0.05$; **, $P < 0.01$; ***, $P < 0.001$; ****, $P < 0.0001$, comparisons between the corpus and antrum using two-way ANOVA, Šídák multiple-comparison test.

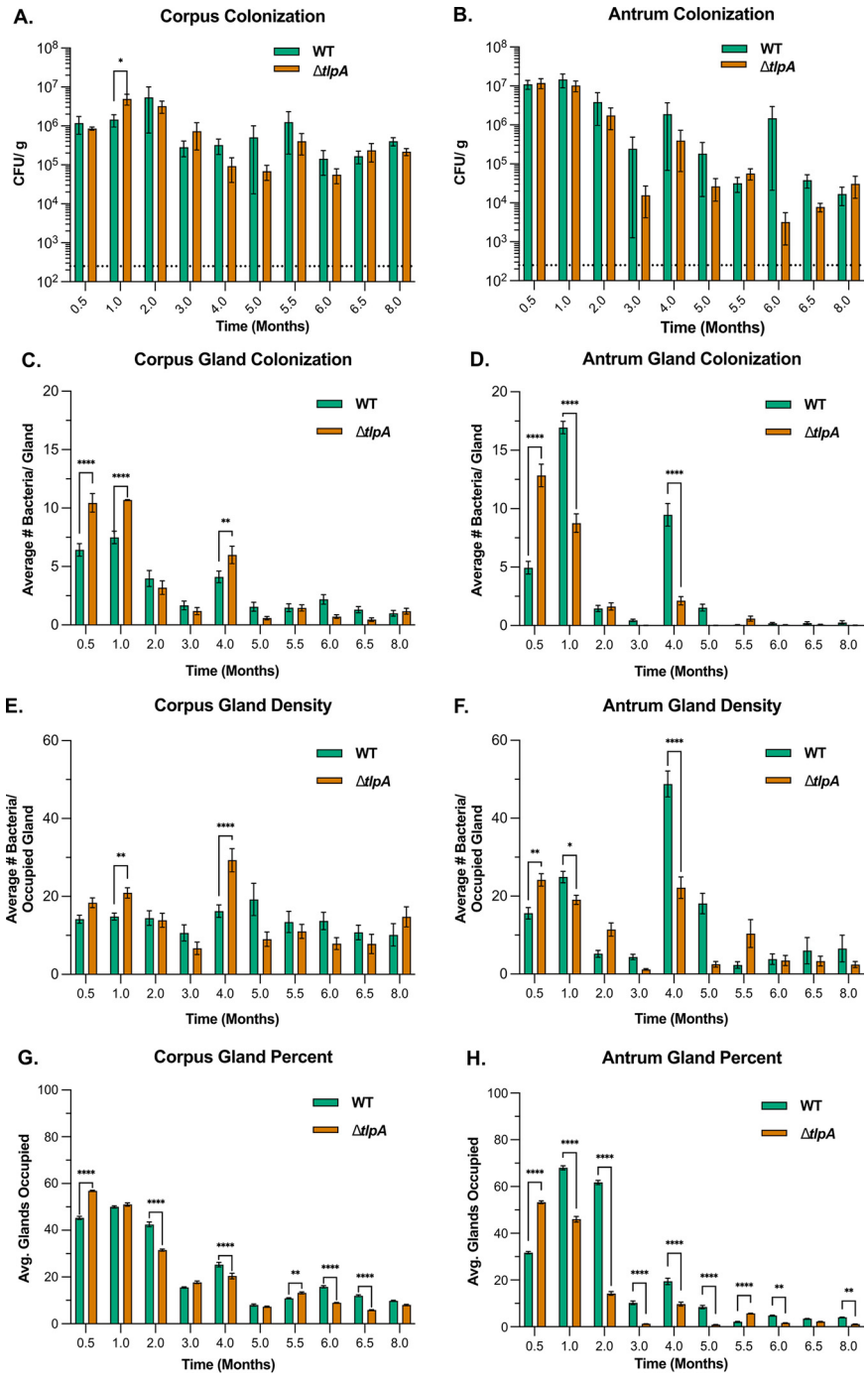

FIG 5 Δ*tlpA H. pylori* occupies more glands, with greater density, during early infection and colonizes glands with lower frequency during late infection. Overall colonization and gland colonization phenotypes were quantified and compared between WT SS1 GFP$^+$ and Δ*tlpA* SS1 GFP$^+$ strains from the infection groups from the same mice as in Fig. 4. (A, C, E, and G) Colonization of WT SS1 and Δ*tlpA* strains in the corpus was assessed for total colonization (A), gland colonization (C), gland density (E), and gland percent (G). (B, D, F, and H) Colonization of WT SS1 and Δ*tlpA* strains in the antrum was assessed for total colonization (B), gland colonization (D), gland density (F), and gland percent (H). For all graphs, error bars represent the standard error of the mean. *, $P < 0.05$; **, $P < 0.01$; ***, $P < 0.001$; ****, $P < 0.0001$, comparisons between strains using two-way ANOVA, Šídák multiple-comparison test.

Overall, these results demonstrate that the Δ*tlpA H. pylori* gland colonization pattern has two main differences from that of the WT. The most striking occurred at early times, when the Δ*tlpA* mutant had higher gland colonization than did the WT in both the corpus and the antrum (Fig. 5B and F). The corpus gland colonization was higher at

0.5 and 1 months, while the antrum was higher only at 0.5 months. In later infection, however, the Δ*tlpA* mutant gland colonization was generally below that of the WT (Fig. 5; Fig. S5).

DISCUSSION

In this work, we sought to understand how *H. pylori* influences inflammation. Our study built on an earlier observation that Δ*tlpA* mutants have elevated late-infection inflammation (33). Here, we report that inflammation induced by Δ*tlpA* mutants is more complex than previously appreciated. Interestingly, we found that *tlpA* mutants and the WT display inflammation that fluctuates, with the *tlpA* mutant inflammation out of phase from that of the WT. This out-of-phase variation gave rise to times when *tlpA* mutant inflammation was either higher or lower than that of the WT. This outcome occurred most dominantly in the mouse corpus; the antrum, in contrast, displayed less variation and similar inflammation levels between the WT and the *tlpA* mutant.

We characterized the Δ*tlpA* mutant immune response using flow cytometry. We observed that Δ*tlpA H. pylori*-infected mice had increased density of Th17 cells (Fig. 3B), but not of any other cell type, during the period of increased inflammation at 5 months postinfection (Fig. 2 and Fig. 3A and C). Th17 cells play a major role in inflammation development during *H. pylori* colonization, primarily through the production of proinflammatory cytokines (51–53). Some of the primary cytokines include the following: (i) IL-17A, which promotes neutrophil recruitments through IL-8 and promotes the expression of antimicrobial peptides from epithelial cells; (ii) IL-17F, which upregulates the expression of other proinflammatory cytokines and chemokines, inducing IL-2, transforming growth factor beta (TGF-β), IL-6, and granulocyte-macrophage colony-stimulating factor (GM-CSF); (iii) IL-21, which promotes the proliferation of Th1 and Th17 cells, creating a positive feedback loop, and promotes the proliferation of B cells; and (iv) IL-22, which acts on nonhematopoietic cells by upregulating antimicrobial peptide expression and promoting tissue repair (51). Interestingly, recent work has shown that arginine, a TlpA chemoattractant (25), and the polyamine pathway are critical for maintaining Th17 pathogenicity (54). Both of these factors drive Th17 cells toward a proinflammatory state. One idea is that WT *H. pylori* uses TlpA to mediate a chemoattractant response toward arginine, allowing *H. pylori* to readily use this amino acid and thus limit its availability to the host. This usage, in turn, could reduce arginine uptake by Th17 cells, resulting in decreased cytokine production and pathogenicity (54).

We also observed significantly higher eosinophil recruitment than that by the WT at multiple time points in Δ*tlpA H. pylori*-infected animals (Fig. 2A). Recently, eosinophils have been shown to play an important role during *H. pylori* colonization, as eosinophils interact with *H. pylori* in the gastric mucosa, regulating Th1 cell proliferation (39). Th1 cells are a significant contributor to the development of pathologies that are observed during *H. pylori* colonization through the production of IFN-γ (45). However, changes in eosinophil populations do not correlate with any change in Th1 recruitment during the period of observation at the 5- to 8-month-postinfection window (Fig. 2A and Fig. 3), suggesting a more dominant role for the Th17 cell population in *tlpA* mutant inflammation.

In this study, our latest time point was at 8 months postinfection. However, as in the human stomach, *H. pylori* can establish chronic colonization, lasting for over a year in a murine model. Colonization studies up to 15 months after infection with *H. pylori* SS1 have been performed, showing that mice colonized for 15 months had higher inflammation than at 6 months postinfection (55). Given this outcome, it would be interesting to see how inflammation evolves over a more extended period and whether periodic fluctuations continue.

Our data suggest that TlpA is important for causing consistent levels of inflammation in the stomach. Keeping inflammation at a low level is important for colonization maintenance. Following the inflammatory spike in the *tlpA* mutant at 5 months postinfection, we observed ~7- and ~17-fold colonization decreases in the corpus and antrum, respectively. It has been well established in the literature that inflammation

severity and colonization levels are inversely related (36, 56, 57). Thus, one idea is that there is an inverse relationship with high numbers of T cells, perhaps at specific glands, resulting in lowered *H. pylori* numbers. Our flow cytometry approach prevented gathering this type of spatial information, and thus, this idea will have to be examined in the future. The results agree with the idea that it is advantageous for *H. pylori* to limit the amount of inflammation it induces during infection.

Over the past decade, it has become appreciated that chemotaxis plays distinct roles in *H. pylori* colonization, necessitating more fine dissection of corpus, antrum, and gastric glands. Initial work focused on CFU levels of *tlpA* mutants. Andermann et al. analyzed CFU in the total stomach, reporting that *tlpA* mutants colonized male FVB/N mice in a manner that was not different from that of the WT after 2 weeks of infection (34). Similar findings were subsequently reported in C57BL/6N mice after 3 or 6 months of infection (33). Subsequent work used the FVB/N mouse strain but separated the corpus and antrum. This work identified that the *tlpA* mutants had a significant, ~5-fold antral CFU defect but none in the corpus (35). In the current work, a different mouse strain was used, again identifying slight antral defects associated with loss of *tlpA* but elevations in the corpus (Fig. 5A). Thus, it seems that colonization defects can be masked when the tissue is not divided and that there appear to be some mouse-specific variations that differentially impact strains lacking *tlpA*.

One important difference between previous work described above and this study is the *tlpA* mutant used. This work relied on an unmarked *tlpA* deletion instead of one with a *cat* insertion. This approach reduces the possibility of polar effects of the *tlpA* mutation and provides a strong independent confirmation of *tlpA*-associated phenotypes, which is important because attempts to create a strain with complementation of *tlpA* in strain SS1 were unsuccessful. However, this lack of complementation is a limitation of the work, along with the fact that animals cannot be followed longitudinally and are sacrificed at each time point. To overcome the latter, we used group sizes of 7 mice to capture within-time-point variability.

More recent work has determined that chemotaxis is critical for gland colonization. Nonchemotactic mutants, including Δ*cheY* and Δ*chepep* mutants, have severe defects in gland colonization compared to WT *H. pylori* during the first month of infection (8, 17, 31, 32, 47). These mutants are fully nonchemotactic, meaning they are unable to detect any receptor input. Mutants that lack specific chemoreceptors also have infection phenotypes but are generally not as severe in terms of CFU or glands. Each chemoreceptor expressed by *H. pylori* is responsible for sensing multiple ligands and signals (19). Accordingly, progress has been made to understand how chemoreceptors regulate the localization of *H. pylori* in the stomach. Studies with the chemoreceptor TlpD are illustrative of the roles that individual chemoreceptors can play. Δ*tlpD H. pylori* has overall colonization defects in the stomach (35), associated with a decrease in the percentage of glands colonized but, interestingly, higher bacterial numbers per gland. This colonization phenotype is ameliorated in mice defective in reactive oxygen species (ROS) production, consistent with TlpD's reported role in sensing and initiating a chemorepellent response to ROS (26, 31). In addition to ROS, TlpD has been shown to sense pH synergistically with TlpA. Δ*tlpAD H. pylori* has a more severe overall colonization defect at 2 weeks postinfection than Δ*tlpD H. pylori* and is defective in gland colonization. These defects were improved via treatment with omeprazole, a proton pump inhibitor that increases the pH of the stomach (28). In total, this work demonstrates the importance of the role that chemoreceptors can play during colonization. The inability to sense specific signals in the gastric environment leads to altered localization, leaving *H. pylori* susceptible to nonoptimal or even toxic host conditions and immune responses.

Our studies examined the colonization patterns of both WT and Δ*tlpA H. pylori* throughout a long-term infection. We found that WT and Δ*tlpA H. pylori* strains have similar overall colonization trends within the corpus and antrum. Both strains favor the antrum during the first month of colonization, but the *tlpA* mutant achieves higher

gland colonization (Fig. 4A and E). After this point, there are no statistical differences in overall colonization between regions of the stomach when analyzing each strain independently. Δ*tlpA H. pylori* favors corpus glands throughout the infection time course, except at 0.5 months postinfection (Fig. 4F and G). The WT, however, tends to favor antral glands 1 to 2 months postinfection, with either higher gland percent or higher density (Fig. 4B to D). Thus, it seems that loss of *tlpA* results in strains that are less able to thrive in the antrum and more able to thrive in the corpus. It is possible that TlpA's signals—arginine, cysteine, and fumarate (25)—are critical in the antral glands and therefore that *tlpA* mutants cannot access these ligands efficiently and do not grow as well as the WT.

Intriguing to note, TlpA appears to be under selective pressure, accumulating a high frequency of mutations in its dCache sensing domain during human infection (58). Of note, these infections were both *cag* PAI$^+$ and *cag* PAI$^-$, indicating *tlpA* is important in both settings. While it is not yet known how these mutations affect TlpA sensing and signaling, it is interesting that *tlpA* is one of the more highly affected loci and may be subject to mutations that change its properties and possible inflammation control abilities.

There is accumulating evidence that *H. pylori* gland colonization is correlated with inflammation. Nonchemotactic *H. pylori* mutants colonize the glands poorly within the first month and induce low inflammation levels at 2 months postinfection, which are characterized by a decreased Th17 response (32, 46). In contrast, our results show that Δ*tlpA H. pylori* has high gland colonization in the corpus until 1 month postinfection, characterized by increased gland density and gland percent relative to those of the WT (Fig. 5B to D). A potential mechanism by which chemotaxis affects inflammatory outcomes is through controlling colonization of gastric glands during the acute stage of infection. During this period, various myeloid cell types in the stomach interact with *H. pylori*. This is critical for developing the effector T-cell response, characterized by the recruitment and proliferation of the proinflammatory Th1 and Th17 cells and the anti-inflammatory Tregs during infection (18). It is plausible that situations that result in high numbers of bacteria per gland increase the chance for total or specific myeloid cells to interact with *H. pylori*. High or distinct myeloid sampling might, in turn, result in differences in T-cell priming and subsequent T-cell populations. On the other hand, nonchemotactic mutants have low gland density and occupancy compared to those of the WT (32). As a result, there may be decreased T-cell priming during the early stage of infection, potentially explaining why nonchemotactic *H. pylori* induces a dampened Th17 response during infection (46).

MATERIALS AND METHODS

Bacterial strains and culture conditions. *H. pylori* strains used in this study were all derived from the *H. pylori* strain SS1. They include WT, WT GFP$^+$, Δ*tlpA* GFP$^+$ (this study), and Δ*tlpA*::*kan-sac* (32, 59, 60). Bacteria were grown at 37°C under microaerobic conditions of 5% O_2, 10% CO_2, and 85% N_2 on solid medium containing Columbia blood agar base (BD), containing 5% defibrinated horse blood (Hemostat Laboratories, Dixon, CA), 50 μg/mL cycloheximide (VWR), 10 μg/mL vancomycin, 5 μg/mL cefsulodin, 2.5 and U/mL polymyxin B (all from Gold Biotechnology), and 0.2% (wt/vol) beta-cyclodextrin (Spectrum Labs, Gardena, CA) (CHBA) or in *Brucella* broth (BD BBL/Fisher) with 10% heat-inactivated fetal bovine serum (FBS) (Life Technologies) (BB10), with shaking. Chloramphenicol-resistant mutants were selected using 10 μg/mL chloramphenicol (Gold Biotechnology) on CHBA, as previously described (34).

The Δ*tlpA* SS1 clean deletion mutant was made for this work by natural transformation of SS1 with pTA12 to create Δ*tlpA*::*kan-sac H. pylori* SS1 and subsequent transformation with pTA14. pTA14 contains an unmarked *tlpA* deletion that leaves the region coding for 14 amino acids at the 5′ end and 19 amino acids at the 3′ end of *tlpA*, flanked by 500 bp of the up- and downstream regions of *tlpA* (60). Sucrose-resistant colonies were selected on CHBA containing 75 μg/mL sucrose (Fisher Chemical), followed by screening for kanamycin sensitivity on CHBA with 15 μg/mL kanamycin (Gold Biotechnology). The Δ*tlpA* deletion was confirmed via PCR (TlpA_SS1_5′, TTGTCTAAAGGTTTGAGTATC; TlpA_SS1_3′, TTAAAACTG CTTTTTATTCAC) (data not shown) and Western blotting using anti-TlpA22 (33) (see Fig. S6 in the supplemental material). Δ*tlpA* SS1 was then transformed with the GFP expression plasmid pTM115 (*ureA*$_p$-GFP *aphA3* Km^r) (32). Colonies were screened for kanamycin resistance and GFP$^+$ fluorescence.

Ethics statement. The University of California Santa Cruz Institutional Animal Care and Use Committee approved all animal protocols and experiments performed (protocol Ottek1804). Female

C57BL/6N mice (*Helicobacter* free; Charles River) were housed and cared for at the University of California Santa Cruz Vivarium.

Animal infections. Female C57BL/6N mice (*Helicobacter* free; Charles River) were orally infected with *H. pylori* at 6 to 8 weeks of age, as done previously (8, 31). This method was chosen based on previous success, because it closely mimics the natural route of infection and because it is less likely than gavage to possibly damage the upper gastrointestinal (GI) tract (8, 31). *H. pylori* SS1 strains were grown to late exponential phase (optical density at 600 nm [OD_{600}] = ~0.75) in BB10 and were checked for GFP fluorescence and motility using a Nikon Eclipse E600 phase-contrast microscope at ×400 magnification with a light-emitting diode (LED) illuminator (pE-300^{white}, CoolLED) with a fluorescent filter for GFP. Motile GFP^+ cultures were concentrated to an OD_{600} of 3 (~9×10^8 CFU/mL) by centrifugation of 1-mL culture aliquots in 1.5-mL Eppendorf tubes at 2,320 × *g* for 10 min. Culture supernatant was removed via aspiration, and pellets were gently resuspended in BB10 to achieve an OD_{600} of 3. For infection, mice were scruffed and oriented at 45° with head and abdomen up and then orally fed 50 μL of the culture with the OD_{600} value of 3 via a pipette tip, for an inoculum of 4.5×10^7 CFU. Mice in the uninfected group were fed 50 μL of BB10. Input inocula were plated on CHBA plates to determine the true input CFU. Two independent time course infections were performed for this study. The infection time course reported in Fig. 1 to 5 included time points at 0.5 (WT and Δ*tlpA*, *n* = 7), 1 (WT and Δ*tlpA*, *n* = 7), 2 (WT and Δ*tlpA*, *n* = 4), 3 (WT and Δ*tlpA*, *n* = 4), 4 (WT and Δ*tlpA*, *n* = 7), 5 (WT, *n* = 7; Δ*tlpA*, *n* = 9), 5.5 (WT, *n* = 7; Δ*tlpA*, *n* = 9), 6 (WT, *n* = 7; Δ*tlpA*, *n* = 8), 6.5 (WT, *n* = 7; Δ*tlpA*, *n* = 8), and 8 (WT and Δ*tlpA*, *n* = 6) months. The infection time course reported in Fig. 1 and 5 and Fig. S5 and S6 included 2 (WT and Δ*tlpA*, *n* = 7), 3 (WT and Δ*tlpA*, *n* = 7), 4 (WT and Δ*tlpA*, *n* = 6), 5 (WT and Δ*tlpA*, *n* = 6), 6 (WT and Δ*tlpA*, *n* = 7), and 8 (WT, *n* = 7; Δ*tlpA*, *n* = 9) months. From this time course, only 3 mice were used for gland analysis from 2 to 5 months postinfection, after which all mice from the infection group were used. For both time course infections, 3 to 4 uninfected mice were included per time point. After the infection period, the mice were sacrificed by CO_2 narcosis, and the stomach was removed at the stomach-esophageal junction and the antrum-duodenum sphincter and then opened by cutting along the lesser curvature of the stomach. Stomach contents were washed gently using ice-cold phosphate-buffered saline (PBS). For dissection, a piece of tissue from the antrum to corpus was removed and stored in a histology cassette (Histoware) with sponge pads in buffered Formalde-Fresh solution (Fisher Chemical) for histology. The remaining stomach was then separated between the antrum and corpus at the transition zone, based on tissue coloration. Each section was then divided into pieces to determine output CFU, to assess gland colonization, and for flow cytometry. To determine colonization load, tissue pieces were weighed, homogenized using the Bullet Blender (Next Advance) with 1.0-mm zirconium silicate beads, and then plated onto CHBA plates, supplemented with 20 μg/mL bacitracin, 10 μg/mL nalidixic acid, and 15 μg/mL kanamycin, to determine CFU per gram of stomach tissue.

Gland isolation and microscopy. Gastric glands from the antrum and corpus were isolated, and *H. pylori* colonization within glands was quantified using the Bacterial Localization in Isolated Glands methods, as done previously (31, 32). Briefly, glands were isolated by agitating dissected tissue from the antrum or corpus in PBS with 5 mM EDTA at 4°C for 2 h. The incubated tissue was then transferred to PBS with 1% sucrose and 1.5% sorbitol (both Fisher Chemical) and mixed vigorously by hand for 30 s. Glands were labeled with 10 μg/mL Hoechst DNA stain (Life Technologies) and stored on ice. Glands were visualized with a Nikon Eclipse E600 microscope with a LED illuminator (pE-300^{white}, CoolLED) and fluorescent filters for 4′,6-diamido-2-phenylindole (DAPI) and GFP. At each infection time point, 100 glands from the antrum and 100 from the corpus were imaged and the number of GFP^+ *H. pylori* bacteria per gland was manually counted. Gland colonization was calculated as the average number of bacteria per gland. Gland density was calculated by averaging the number of bacteria within occupied glands. Gland percent is calculated as the average frequency of glands occupied per mouse. Standard error of the mean was calculated for each. Statistical analysis of the data for comparisons between infection groups or stomach regions at each time point was performed using two-way analysis of variance (ANOVA), Šídák multiple-comparison test.

Histology. Tissue pieces from the antrum to corpus stored in buffered Formalde-Fresh solution (Fisher Chemical) in histology cassettes with sponges were processed for sectioning and graded for lymphatic infiltration as done previously (33). Briefly, tissue was embedded in paraffin, sectioned (5 μm), stained in hematoxylin and eosin, and evaluated by a pathologist in a blind fashion (J. Elliot Carter). To ensure reproducibility, slides were read twice and checked to ensure identical grades were obtained. Inflammation, defined as lymphocytic infiltration, was assessed using standard methods (33, 61), and sections were given scores as follows: 0, no infiltrate; 1, mild, multifocal infiltration; 2, mild, widespread infiltration; 3, mild, widespread and moderate, multifocal infiltration; 4, moderate, widespread infiltration; and 5, moderate, widespread and severe, multifocal infiltration. Neutrophil infiltration was scored as present or absent. Sections were also assessed for atrophy according to previously defined standards (62). Rugge et al. (62) defined gastric atrophy as the loss of gastric glands in the area of the gastric mucosa being sampled. Atrophy can be associated with metaplasia, where gastric glands from a section of stomach are lost and replaced by gastric glands from a separate region of the gastric mucosa, or as atrophy without metaplasia, in which gastric glands from a section of stomach are lost with no replacement by other gastric glands and fibrosis of the lamina propria is seen. Samples negative for atrophy lack either manifestation of atrophy described and also lack metaplasia and hyperplasia. Mice from both time course infections were pooled for analysis. The average inflammation grade and standard error of the mean were calculated for each strain per time point. Statistical analysis of the data between strains was performed using two-way ANOVA, Šídák multiple-comparison test.

Gastric lamina propria leukocyte isolation. Lamina propria leukocyte isolation from gastric tissue was performed as done previously (39, 40, 63). Tissue pieces from the antrum and corpus were placed in 50-mL conical tubes in 5 mL RPMI (Gibco) with 10% FBS (Gibco) on ice during the dissection of the mice. Medium was discarded by aspiration and replaced by 30 mL of 1× Hanks balanced salt solution (Gibco) with 0.5% bovine serum albumin (BSA) (Millipore Sigma) and 5 mM EDTA (Fisher Chemical) prewarmed to 37°C. The tubes were then incubated horizontally at 37°C with shaking for 1 h at 200 rpm in a Thermo Scientific MaxQ 4000 benchtop orbital shaker. After incubation, the supernatant was removed by aspiration, the tissue was resuspended in 30 mL of room-temperature PBS for 2 min, and then the PBS was replaced with 15 mL of RPMI medium with 10% fetal calf serum (FCS), 500 U/mL type IV collagenase (Sigma-Aldrich), and 0.05 mg/mL DNase I (Gold Biotechnology) prewarmed to 37°C and incubated horizontally at 37°C with shaking for 1 h at 200 rpm in a Thermo Scientific MaxQ 4000 benchtop orbital shaker. Following incubation, the solution was pulled through a 200-mL syringe 10 to 15 times to finish homogenization. The supernatant containing lamina propria leukocytes was filtered through a 40-μm cell strainer (Falcon), and then 30 mL of PBS was added. Cells were collected by centrifugation in a Thermo Scientific Sorvall Legend XTR with a TX-1000 rotor at 1,500 rpm (526 × *g*) for 8 min, the supernatant was discarded by aspiration, and the cell pellet was resuspended in 4 mL of 80% Percoll (GE Healthcare), added to a 15-mL Falcon tube, and then overlaid with 4 mL of 40% Percoll. The 40/80% Percoll gradient was centrifuged for 15 min at 3,000 rpm at 18°C. The interphase, containing cells, was collected and washed with PBS with 0.5% BSA.

Flow cytometry. Flow cytometry was carried out as described previously (39, 40, 63). For surface staining, cells were stained in PBS with 0.5% BSA with fixable viability dye eFluor 780 (eBioscience) and a combination of the following antibodies: anti-mouse CD45 (phycoerythrin [PE]/Cy5, 30-F11, BioLegend), CD45 (Alexa Fluor 700, 30-F11, BioLegend), CD11c (allophycocyanin [APC], N418, BioLegend), I-A/I-E (Alexa Fluor 700, M5/114.15.2, BioLegend), F4/80 (fluorescein isothiocyanate [FITC], BM8, BioLegend), CD103 (Brilliant Violet 605, 2E7, BioLegend), CD11b (Brilliant Violet 421, M1/70, BioLegend), Ly-6G (PE/Dazzle 594, 1A8, BioLegend), Ly-6C (PE/Cy7, HK1.4, BioLegend), Siglec-F (PE, S17007C, BioLegend), TCRβ (PE/Cy7, H57-597, BD), or CD4 (APC, RM4-5, BioLegend). Mouse Fc block (CD16/CD32, BD) was used to minimize unspecific antibody binding. For transcription factor staining, cells were fixed and permeabilized with the FoxP3 Fix/Perm buffer set (BioLegend) following the manufacturer's instructions. Cells were stained with anti-mouse T-Bet (FITC, 4B10, BioLegend), RORγT (PE, Q31-378, BD), and FoxP3 (Pacific Blue, BioLegend, MF-14). Absolute cell counts were determined by adding CountBright Plus absolute counting beads (Invitrogen) to each sample, which was analyzed on an LSRII flow cytometer (BD Biosciences). Up to 300,000 cells were recorded per mouse, with some samples containing as few as 30,000 cells. Absolute counts are reported at cells per microliter. Analysis was performed using FlowJo (BD).

SUPPLEMENTAL MATERIAL

Supplemental material is available online only.

SUPPLEMENTAL FILE 1, PDF file, 1.8 MB.

ACKNOWLEDGMENTS

We thank Martha Zuñiga, Vicki Auerbuch Stone, and Fitnat Yildiz for their thoughtful comments on the manuscript. We thank Bari Holm Nazario and the UCSC Institute for the Biology of Stem Cells Flow Cytometry Facility for technical support and training (RRID: SCR_021149).

The described project was supported by the National Institute of Allergy and Infectious Diseases (NIAID) grant RO1AI116946 to K.M.O. The funders had no role in study design, data collection, and interpretation, or decision to submit the work for publication.

REFERENCES

1. Harris PR, Smythies LE, Smith PD, Perez-Perez GI. 2013. Role of childhood infection in the sequelae of *H. pylori* disease. Gut Microbes 4:426–438. https://doi.org/10.4161/gmic.26943.
2. Salama NR, Hartung ML, Müller A. 2013. Life in the human stomach: persistence strategies of the bacterial pathogen *Helicobacter pylori*. Nat Rev Microbiol 11:385–399. https://doi.org/10.1038/nrmicro3016.
3. Cover TL, Blaser MJ. 2009. *Helicobacter pylori* in health and disease. Gastroenterology 136:1863–1873. https://doi.org/10.1053/j.gastro.2009.01.073.
4. Arnold IC, Dehzad N, Reuter S, Martin H, Becher B, Taube C, Müller A. 2011. *Helicobacter pylori* infection prevents allergic asthma in mouse models through the induction of regulatory T cells. J Clin Invest 121:3088–3093. https://doi.org/10.1172/JCI45041.
5. Ferlay J, Soerjomataram I, Dikshit R, Eser S, Mathers C, Rebelo M, Parkin DM, Forman D, Bray F. 2015. Cancer incidence and mortality worldwide: sources, methods and major patterns in GLOBOCAN 2012. Int J Cancer 136:E359–E386. https://doi.org/10.1002/ijc.29210.
6. Hooi JKY, Lai WY, Ng WK, Suen MMY, Underwood FE, Tanyingoh D, Malfertheiner P, Graham DY, Wong VWS, Wu JCY, Chan FKL, Sung JJY, Kaplan GG, Ng SC. 2017. Global prevalence of *Helicobacter pylori* infection: systematic review and meta-analysis. Gastroenterology 153:420–429. https://doi.org/10.1053/j.gastro.2017.04.022.
7. Plummer M, Franceschi S, Vignat J, Forman D, de Martel C. 2015. Global burden of gastric cancer attributable to *Helicobacter pylori*. Int J Cancer 136:487–490. https://doi.org/10.1002/ijc.28999.
8. Howitt MR, Lee JY, Lertsethtakarn P, Vogelmann R, Joubert L-M, Ottemann KM, Amieva MR. 2011. ChePep controls *Helicobacter pylori* infection of the gastric glands and chemotaxis in the Epsilonproteobacteria. mBio 2:e00098-11. https://doi.org/10.1128/mBio.00098-11.

9. Keilberg D, Ottemann KM. 2016. How *Helicobacter pylori* senses, targets and interacts with the gastric epithelium: *H. pylori*-gastric epithelium interaction. Environ Microbiol 18:791–806. https://doi.org/10.1111/1462-2920.13222.
10. Schreiber S, Konradt M, Groll C, Scheid P, Hanauer G, Werling H-O, Josenhans C, Suerbaum S. 2004. The spatial orientation of *Helicobacter pylori* in the gastric mucus. Proc Natl Acad Sci U S A 101:5024–5029. https://doi.org/10.1073/pnas.0308386101.
11. Yang C, Ottemann KM. 2019. Control of bacterial colonization in the glands and crypts. Curr Opin Microbiol 47:38–44. https://doi.org/10.1016/j.mib.2018.11.004.
12. Schreiber S, Bucker R, Groll C, Azevedo-Vethacke M, Garten D, Scheid P, Friedrich S, Gatermann S, Josenhans C, Suerbaum S. 2005. Rapid loss of motility of *Helicobacter pylori* in the gastric lumen in vivo. Infect Immun 73:1584–1589. https://doi.org/10.1128/IAI.73.3.1584-1589.2005.
13. Goyal RK, Guo Y, Mashimo H. 2019. Advances in the physiology of gastric emptying. Neurogastroenterol Motil 31:e13546. https://doi.org/10.1111/nmo.13546.
14. Atuma C, Strugala V, Allen A, Holm L. 2001. The adherent gastrointestinal mucus gel layer: thickness and physical state *in vivo*. Am J Physiol Gastrointest Liver Physiol 280:G922–G929. https://doi.org/10.1152/ajpgi.2001.280.5.G922.
15. Schreiber S, Scheid P. 1997. Gastric mucus of the guinea pig: proton carrier and diffusion barrier. Am J Physiol Gastrointest Liver Physiol 272:G63–G70. https://doi.org/10.1152/ajpgi.1997.272.1.G63.
16. Creamer B, Shorter RG, Bamforth J. 1961. The turnover and shedding of epithelial cells: part I. The turnover in the gastro-intestinal tract. Gut 2:110–118. https://doi.org/10.1136/gut.2.2.110.
17. Sigal M, Rothenberg ME, Logan CY, Lee JY, Honaker RW, Cooper RL, Passarelli B, Camorlinga M, Bouley DM, Alvarez G, Nusse R, Torres J, Amieva MR. 2015. *Helicobacter pylori* activates and expands Lgr5+ stem cells through direct colonization of the gastric glands. Gastroenterology 148:1392–1404.e21. https://doi.org/10.1053/j.gastro.2015.02.049.
18. Zhang X, Arnold IC, Müller A. 2020. Mechanisms of persistence, innate immune activation and immunomodulation by the gastric pathogen *Helicobacter pylori*. Curr Opin Microbiol 54:1–10. https://doi.org/10.1016/j.mib.2020.01.003.
19. Johnson KS, Ottemann KM. 2018. Colonization, localization, and inflammation: the roles of *H. pylori* chemotaxis in vivo. Curr Opin Microbiol 41:51–57. https://doi.org/10.1016/j.mib.2017.11.019.
20. Lertsethtakarn P, Ottemann KM, Hendrixson DR. 2011. Motility and chemotaxis in *Campylobacter* and *Helicobacter*. Annu Rev Microbiol 65:389–410. https://doi.org/10.1146/annurev-micro-090110-102908.
21. Cerda O, Rivas A, Toledo H. 2003. *Helicobacter pylori* strain ATCC700392 encodes a methyl-accepting chemotaxis receptor protein (MCP) for arginine and sodium bicarbonate. FEMS Microbiol Lett 224:175–181. https://doi.org/10.1016/S0378-1097(03)00423-3.
22. Cerda OA, Núñez-Villena F, Soto SE, Ugalde JM, López-Solís R, Toledo H. 2011. tlpA gene expression is required for arginine and bicarbonate chemotaxis in *Helicobacter pylori*. Biol Res 44:277–282. https://doi.org/10.4067/S0716-97602011000300009.
23. Huang JY, Sweeney EG, Sigal M, Zhang HC, Remington SJ, Cantrell MA, Kuo CJ, Guillemin K, Amieva MR. 2015. Chemodetection and destruction of host urea allows *Helicobacter pylori* to locate the epithelium. Cell Host Microbe 18:147–156. https://doi.org/10.1016/j.chom.2015.07.002.
24. Machuca MA, Johnson KS, Liu YC, Steer DL, Ottemann KM, Roujeinikova A. 2017. *Helicobacter pylori* chemoreceptor TlpC mediates chemotaxis to lactate. Sci Rep 7:14089. https://doi.org/10.1038/s41598-017-14372-2.
25. Johnson KS, Elgamoudi BA, Jen FE-C, Day CJ, Sweeney EG, Pryce ML, Guillemin K, Haselhorst T, Korolik V, Ottemann KM. 2021. The dCache chemoreceptor TlpA of *Helicobacter pylori* binds multiple attractant and antagonistic ligands via distinct sites. mBio 12:e01819-21. https://doi.org/10.1128/mBio.01819-21.
26. Collins KD, Andermann TM, Draper J, Sanders L, Williams SM, Araghi C, Ottemann KM. 2016. The *Helicobacter pylori* CZB cytoplasmic chemoreceptor TlpD forms an autonomous polar chemotaxis signaling complex that mediates a tactic response to oxidative stress. J Bacteriol 198:1563–1575. https://doi.org/10.1128/JB.00071-16.
27. Croxen MA, Sisson G, Melano R, Hoffman PS. 2006. The *Helicobacter pylori* chemotaxis receptor TlpB (HP0103) is required for pH taxis and for colonization of the gastric mucosa. J Bacteriol 188:2656–2665. https://doi.org/10.1128/JB.188.7.2656-2665.2006.
28. Huang JY, Goers Sweeney E, Guillemin K, Amieva MR. 2017. Multiple acid sensors control *Helicobacter pylori* colonization of the stomach. PLoS Pathog 13:e1006118. https://doi.org/10.1371/journal.ppat.1006118.
29. Perkins A, Tudorica DA, Amieva MR, Remington SJ, Guillemin K. 2019. *Helicobacter pylori* senses bleach (HOCl) as a chemoattractant using a cytosolic chemoreceptor. PLoS Biol 17:e3000395. https://doi.org/10.1371/journal.pbio.3000395.
30. Schweinitzer T, Mizote T, Ishikawa N, Dudnik A, Inatsu S, Schreiber S, Suerbaum S, Aizawa S-I, Josenhans C. 2008. Functional characterization and mutagenesis of the proposed behavioral sensor TlpD of *Helicobacter pylori*. J Bacteriol 190:3244–3255. https://doi.org/10.1128/JB.01940-07.
31. Collins KD, Hu S, Grasberger H, Kao JY, Ottemann KM. 2018. Chemotaxis allows bacteria to overcome host-generated reactive oxygen species that constrain gland colonization. Infect Immun 86:e00878-17. https://doi.org/10.1128/IAI.00878-17.
32. Keilberg D, Zavros Y, Shepherd B, Salama NR, Ottemann KM. 2016. Spatial and temporal shifts in bacterial biogeography and gland occupation during the development of a chronic infection. mBio 7:e01705-16. https://doi.org/10.1128/mBio.01705-16.
33. Williams SM, Chen Y-T, Andermann TM, Carter JE, McGee DJ, Ottemann KM. 2007. *Helicobacter pylori* chemotaxis modulates inflammation and bacterium-gastric epithelium interactions in infected mice. Infect Immun 75:3747–3757. https://doi.org/10.1128/IAI.00082-07.
34. Andermann TM, Chen Y-T, Ottemann KM. 2002. Two predicted chemoreceptors of *Helicobacter pylori* promote stomach infection. Infect Immun 70:5877–5881. https://doi.org/10.1128/IAI.70.10.5877-5881.2002.
35. Rolig AS, Shanks J, Carter JE, Ottemann KM. 2012. *Helicobacter pylori* requires TlpD-driven chemotaxis to proliferate in the antrum. Infect Immun 80:3713–3720. https://doi.org/10.1128/IAI.00407-12.
36. Arnold IC, Lee JY, Amieva MR, Roers A, Flavell RA, Sparwasser T, Müller A. 2011. Tolerance rather than immunity protects from *Helicobacter pylori*-induced gastric preneoplasia. Gastroenterology 140:199–209.e8. https://doi.org/10.1053/j.gastro.2010.06.047.
37. White JR, Winter JA, Robinson K. 2015. Differential inflammatory response to *Helicobacter pylori* infection: etiology and clinical outcomes. J Inflamm Res 8:137–147. https://doi.org/10.2147/JIR.S64888.
38. Wroblewski LE, Peek RM, Wilson KT. 2010. *Helicobacter pylori* and gastric cancer: factors that modulate disease risk. Clin Microbiol Rev 23:713–739. https://doi.org/10.1128/CMR.00011-10.
39. Arnold IC, Artola-Borán M, Tallón de Lara P, Kyburz A, Taube C, Ottemann K, van den Broek M, Yousefi S, Simon H-U, Müller A. 2018. Eosinophils suppress Th1 responses and restrict bacterially induced gastrointestinal inflammation. J Exp Med 215:2055–2072. https://doi.org/10.1084/jem.20172049.
40. Arnold IC, Zhang X, Urban S, Artola-Borán M, Manz MG, Ottemann KM, Müller A. 2017. NLRP3 controls the development of gastrointestinal CD11b+ dendritic cells in the steady state and during chronic bacterial infection. Cell Rep 21:3860–3872. https://doi.org/10.1016/j.celrep.2017.12.015.
41. Oertli M, Sundquist M, Hitzler I, Engler DB, Arnold IC, Reuter S, Maxeiner J, Hansson M, Taube C, Quiding-Järbrink M, Müller A. 2012. DC-derived IL-18 drives Treg differentiation, murine *Helicobacter pylori*-specific immune tolerance, and asthma protection. J Clin Invest 122:1082–1096. https://doi.org/10.1172/JCI61029.
42. Lundgren A, Trollmo C, Edebo A, Svennerholm A-M, Lundin BS. 2005. *Helicobacter pylori*-specific $CD4^+$ T cells home to and accumulate in the human *Helicobacter pylori*-infected gastric mucosa. Infect Immun 73:5612–5619. https://doi.org/10.1128/IAI.73.9.5612-5619.2005.
43. Bamford KB, Fan X, Crowe SE, Leary JF, Gourley WK, Luthra GK, Brooks EG, Graham DY, Reyes VE, Ernst PB. 1998. Lymphocytes in the human gastric mucosa during *Helicobacter pylori* have a T helper cell 1 phenotype. Gastroenterology 114:482–492. https://doi.org/10.1016/S0016-5085(98)70531-1.
44. Eaton KA, Mefford M, Thevenot T. 2001. The role of T cell subsets and cytokines in the pathogenesis of *Helicobacter pylori* gastritis in mice. J Immunol 166:7456–7461. https://doi.org/10.4049/jimmunol.166.12.7456.
45. Gray BM, Fontaine CA, Poe SA, Eaton KA. 2013. Complex T cell interactions contribute to *Helicobacter pylori* gastritis in mice. Infect Immun 81:740–752. https://doi.org/10.1128/IAI.01269-12.
46. Rolig AS, Carter JE, Ottemann KM. 2011. Bacterial chemotaxis modulates host cell apoptosis to establish a T-helper cell, type 17 (Th17)-dominant immune response in *Helicobacter pylori* infection. Proc Natl Acad Sci U S A 108:19749–19754. https://doi.org/10.1073/pnas.1104598108.
47. Fung C, Tan S, Nakajima M, Skoog EC, Camarillo-Guerrero LF, Klein JA, Lawley TD, Solnick JV, Fukami T, Amieva MR. 2019. High-resolution mapping reveals that microniches in the gastric glands control *Helicobacter*

pylori colonization of the stomach. PLoS Biol 17:e3000231. https://doi.org/10.1371/journal.pbio.3000231.
48. Terry K, Williams SM, Connolly L, Ottemann KM. 2005. Chemotaxis plays multiple roles during *Helicobacter pylori* animal infection. Infect Immun 73:803–811. https://doi.org/10.1128/IAI.73.2.803-811.2005.
49. Carbo A, Olivares-Villagómez D, Hontecillas R, Bassaganya-Riera J, Chaturvedi R, Piazuelo MB, Delgado A, Washington MK, Wilson KT, Algood HMS. 2014. Systems modeling of the role of interleukin-21 in the maintenance of effector CD4 $^{+}$ T cell responses during chronic *Helicobacter pylori* infection. mBio 5:e01243-14. https://doi.org/10.1128/mBio.01243-14.
50. Martinez LE, O'Brien VP, Leverich C, Knoblaugh SE, Salama NR. 2019. Non-helical *Helicobacter pylori* mutants show altered gland colonization and elicit less gastric pathology than helical bacteria during chronic infection. Infect Immun 87:e00904-18. https://doi.org/10.1128/IAI.00904-18.
51. Dixon BREA, Hossain R, Patel RV, Algood HMS. 2019. Th17 cells in *Helicobacter pylori* infection: a dichotomy of help and harm. Infect Immun 87:e00363-19. https://doi.org/10.1128/IAI.00363-19.
52. Serrano C, Wright SW, Bimczok D, Shaffer CL, Cover TL, Venegas A, Salazar MG, Smythies LE, Harris PR, Smith PD. 2013. Downregulated Th17 responses are associated with reduced gastritis in *Helicobacter pylori*-infected children. Mucosal Immunol 6:950–959. https://doi.org/10.1038/mi.2012.133.
53. Shiomi S, Toriie A, Imamura S, Konishi H, Mitsufuji S, Iwakura Y, Yamaoka Y, Ota H, Yamamoto T, Imanishi J, Kita M. 2008. IL-17 is involved in *Helicobacter pylori*-induced gastric inflammatory responses in a mouse model. Helicobacter 13:518–524. https://doi.org/10.1111/j.1523-5378.2008.00629.x.
54. Wagner A, Wang C, Fessler J, DeTomaso D, Avila-Pacheco J, Kaminski J, Zaghouani S, Christian E, Thakore P, Schellhaass B, Akama-Garren E, Pierce K, Singh V, Ron-Harel N, Douglas VP, Bod L, Schnell A, Puleston D, Sobel RA, Haigis M, Pearce EL, Soleimani M, Clish C, Regev A, Kuchroo VK, Yosef N. 2021. Metabolic modeling of single Th17 cells reveals regulators of autoimmunity. Cell 184:4168–4185.e21. https://doi.org/10.1016/j.cell.2021.05.045.
55. Thompson LJ, Danon SJ, Wilson JE, O'Rourke JL, Salama NR, Falkow S, Mitchell H, Lee A. 2004. Chronic *Helicobacter pylori* infection with Sydney strain 1 and a newly identified mouse-adapted strain (Sydney strain 2000) in C57BL/6 and BALB/c mice. Infect Immun 72:4668–4679. https://doi.org/10.1128/IAI.72.8.4668-4679.2004.
56. Algood HMS, Cover TL. 2006. *Helicobacter pylori* persistence: an overview of interactions between *H. pylori* and host immune defenses. Clin Microbiol Rev 19:597–613. https://doi.org/10.1128/CMR.00006-06.
57. Chen W, Shu D, Chadwick VS. 2001. Reduced colonization of gastric mucosa by Helicobacter pylori in mice deficient in interleukin-10. J Gastroenterol Hepatol 16:377–383. https://doi.org/10.1046/j.1440-1746.2001.02459.x.
58. Ailloud F, Didelot X, Woltemate S, Pfaffinger G, Overmann J, Bader RC, Schulz C, Malfertheiner P, Suerbaum S. 2019. Within-host evolution of Helicobacter pylori shaped by niche-specific adaptation, intragastric migrations and selective sweeps. Nat Commun 10:2273. https://doi.org/10.1038/s41467-019-10050-1.
59. Lee A, O'Rourke J, De Ungria MC, Robertson B, Daskalopoulos G, Dixon MF. 1997. A standardized mouse model of *Helicobacter pylori* infection: introducing the Sydney strain. Gastroenterology 112:1386–1397. https://doi.org/10.1016/S0016-5085(97)70155-0.
60. Rader BA, Wreden C, Hicks KG, Sweeney EG, Ottemann KM, Guillemin K. 2011. *Helicobacter pylori* perceives the quorum-sensing molecule AI-2 as a chemorepellent via the chemoreceptor TlpB. Microbiology (Reading) 157:2445–2455. https://doi.org/10.1099/mic.0.049353-0.
61. Eaton KA, Radin MJ, Krakowka S. 1995. An animal model of gastric ulcer due to bacterial gastritis in mice. Vet Pathol 32:489–497. https://doi.org/10.1177/030098589503200506.
62. Rugge M, Correa P, Dixon MF, Fiocca R, Hattori T, Lechago J, Leandro G, Price AB, Sipponen P, Solcia E, Watanabe H, Genta RM. 2002. Gastric mucosal atrophy: interobserver consistency using new criteria for classification and grading. Aliment Pharmacol Ther 16:1249–1259. https://doi.org/10.1046/j.1365-2036.2002.01301.x.
63. Arnold IC, Zhang X, Artola-Boran M, Fallegger A, Sander P, Johansen P, Müller A. 2019. BATF3-dependent dendritic cells drive both effector and regulatory T-cell responses in bacterially infected tissues. PLoS Pathog 15:e1007866. https://doi.org/10.1371/journal.ppat.1007866.